ZERO PHONON AND PHONON ASSISTED RADIATIVE TRANSITION RATES BASED ON FINITE POTENTIAL WELL APPROXIMATION FOR SILICON NANOCRYSTALLITE EMBEDDED IN SILICON OXIDE

By

Girma Alemgasha

A THESIS SUBMITTED TO THE SCHOOL OF GRADUATES IN PARTIAL FULFILLMENT OF THE REQUIREMENTS FOR THE DEGREE OF MASTER OF SCIENCE IN PHYSICS

AT

ADDIS ABABA UNIVERSITY

JUNE 2009

Table of Contents

List of Figures

Abstract

The purpose of this thesis was to study phonon assisted and zero phonon radiative lifetimes of electron-hole pair which are excited and recombine inside nc-Si, on the basis of more realistic assumption of finite potential well and envelope wave approximations for oxidized PS and nc-Si inside SiO_2. Finite potential well approximation results the spread of conduction and valence band edge wave functions in to SiO_2. Solving time independent Schrödinger equation in the two materials and applying matching boundary condition at the interface for envelope wave function part; we found bandgap energy closer to experimental results that increase at lower rate as we shrink the size of nc-Si compared to infinitely deep potential well approximation. Radiative rates for both zero phonon and phonon assisted transitions are calculated with the newly developed wave functions and by separately calculating momentum overlap factor and incorporating it into momentum matrix elements by hand. New radiative lifetime estimation in the order of nanosecond for nc-Si size below 2 nm is found. We also found μs order of life time for phonon assisted recombination rate below 2 nm size of nc-Si. However, the value we got for phonon assisted radiative transition rate does not show any significant difference from infinitely deep potential well approximation results.

Acknowledgements

Firstly, I would like to thank the ONE who teaches me what I must learn in the course of my life.

Secondly, I would like to express my deep sense of gratitude to my advisor, Dr. Sib Krishna Goshal, for believing in me and patiently pusuing me to keep the schedule and meet the deadlines in completing this thesis. He gave me invaluable guidance, advice and constructive comments.

My gratitude also goes to Derse Gugsa, material science student in Erasmus mundus program, for sending me papers and books that greatly helps me for finalizing this thesis.

Chapter 1

Introduction

1.1 Silicon: From Microelectronics to Optoelectronics

Silicon is a material where ***the extraordinary is made ordinary***[1]. This statement is a reflection of overwhelming dominance of silicon on semiconductor technology, and its enormous contribution to the community over the last decades. Silicon of all semiconductors, underpins nearly all microelectronics today and will continue to do so for some time to come. Compared to Germanium, Silicon is larger bandgap ($1.12eV$) material which allows higher operating temperature and is readily available naturally in large quantities. The other main reason for tremendous success of Si based microelectronics in current semiconductor technonology is its natural oxide (SiO_2). The interface between Si and (SiO_2) is very sharp and contains low trap density ($\approx 10^9 trap/cm^2$). It provides excellent mechanical support with desirable electronic property which we don't normally have for other semiconductor materials like GaAs. Consequently, silicon is a material of choice for fabrication in the current microelectronic industry.

Nowadays, Integration of photonics with electronics is hightly desired to address ever increasing need for smart optical networks, with greater bandwidth and low cost, as well as it is desired to alleviate the interconnect bottleneck imposed on CMOS (compatible metal oxide semiconductor) circuits operating above 10GHz[4]. As a result, large effort is being poured on the development of compact optoelectronic platforms. Though Si is dominant in microelectronic industry, its performance as light emitting device is so limited that compound (III-V) semiconductors are currently used when ever there is a need for photon generation. Nevertheless, compound semiconductor technology has serious drawbacks when we come to large scale production with low cost, and when we see the quality as well as stability of the materials when they are combined with silicon.

Numerous techniques are being investigated by different researchers around the globe to merge si-based electronics with hybride technologies for light emitters and modulators[4]. It is, however, believed that most satisfactory solution would come if optoelectronic and photonic devices are produced entirely from Si-based materials[4]. Common platform of this kind that integrate both photonic and electronic functionalities is a tremendous boost for answering ever increasing demands of faster communications and pervasive computing. The major deficiency in Si-based optoelectronic devices is lack of suitable light emitters and especially lasers. Intrinsic bulk silicon is poor light emitter characterized by slow radiative and fast nonradiative decaying rates of excited electron-hole pairs that results low luminescence efficiency to the level one photon per $\sim 10^6$ excited electron hole pairs at 300K. Turning Si into efficient light emitting device has been very active area of experimental and theoretical research, looking forward to the possible revolutionary scenario in the optoelectronic

technology if it is found to be feasible, i.e. ***to make the extraordinary happen again on silicon***[4].

Various strategies and approaches are suggested by different active workers in this area to alleviate the bottleneck in increasing quantum efficiency with emission wavelength tunability of Si based optical materials. Among suggested strategies the following are the leading frontiers[4]

- Use of $Si_{1-x}Ge_x$ quantum well or Si/Ge superlattice structures
- Band structure engineering
- Quantum confinement effects in low dimensional structures
- Impurity-mediated luminescence, for example, by the addition of rare earth ions.

The problem that is addressed in all approaches is same, i.e. to increase quantum efficiency of silicon and to tune emission wavelength. Of all suggested and actively explored strategies, in this paper, only low dimensional structures particularly silicon nanocrystals and porous silicon are investigated as possible means of turning Si to efficient light emitter.

1.2 Size Effects

1.2.1 Optical Properties of Bulk Silicon

Bulk silicon is generally characterized as poor light emitter with very low luminescence efficiency ($\backsim 10^{-6}$) and slow optical response. Indirect energy band structure of bulk Si (Figure 1.1) is mainly responsible for poor optical performances. Highest point in

valence band maximum occurs at the Brillouin zone center (i.e Γ point or at $\mathbf{K} = 0$ point), and conduction band exhibit its lowest value near the X point at the Brillouin zone boundary (i.e., $(0.85)2\pi/a$) along (001) direction). The momentum difference between these two points is large to be supplied by photon during absorption and emission processes. Therefore, photon absorption and emission in silicon needs third party involvement (i.e., phonon) to meet universal momentum conservation law. Such quite inefficient three-body process increase radiative life time to order of millisecond. This is miserable parameter for bulk silicon when it is compared with nanosecond life time of direct band gap semiconductors like GaAs. To make it more worse, in bulk Si nonradiative relaxation channels nearly monopolize the de-excitation market to the level that doesn't allow us even to observe the dawdling radiative process which is clearly reflected in nearly zero (10^{-6})quantum efficiency. These are central deficiencies of c-Si that needs to be solved first, before we use it as light emitting material and integrate it with conventional microelectronic circuits.

1.2.2 Luminescence property of Silicon Nanomaterials

One way of unravelling the mystery of getting efficient emission of light from Si with significantly improved response time is to make use of low dimensional Si materials. The effects determined by size in nanometer scale pertain to the evolution of structural, thermodynamic, electronic, spectroscopic, electromagnetic and chemical features. Si nanostructure has attracted particular attention from scientific and technological viewpoints as a result of observed valuable properties that could be exploited for optoelectronic applications. Fundamental properties of single

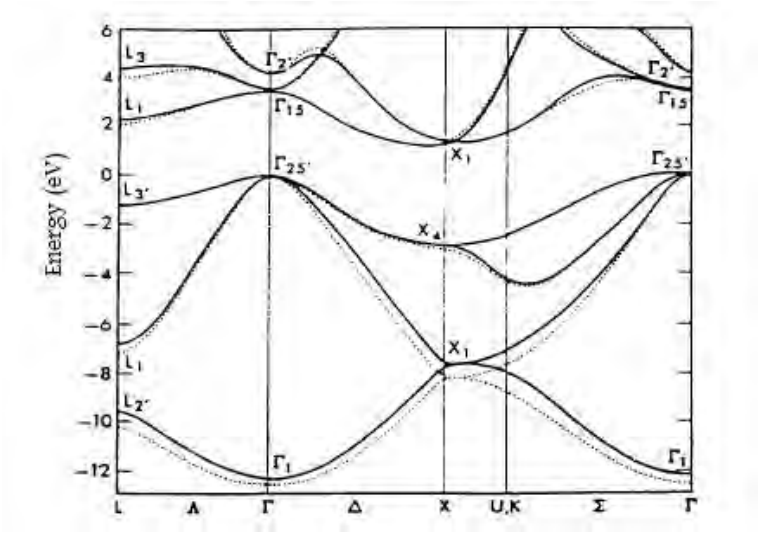

Figure 1.1: Band structure of bulk Si. nonlocal (solid), and local (dashed line) psedopotential calculations.[5]

c-Si(crystalline Silicon-bulk) are substantially modified in nc-Si (nanocrystalline silicon) due to enhanced quantum confinement. Luminescence optical properties of c-Si are considerably modified as we shrink the size scale to nano-level. This, much loved, modification of luminescence characteristics are attributed to several factors, where enhanced quantum confinement, reduction of noneradiative channels, quantization effects on phonon modes, and strong effects from surfaces/interface are the leading factors.

Confinement of carriers in nc-Si leads to several consequences. Quantum dots are generally modelled as extremely small puddle of electrons, which can be assumed as an artificial atom, where the confinement of electrons and holes leads to atomic like quantized levels. The carriers in quantum dot form orbitals much like the electrons in atomic orbital around atomic nucleus. As a result, the density of states for nc-Si or Quantum dots has atomic like nature rather than keeping their bulk form as

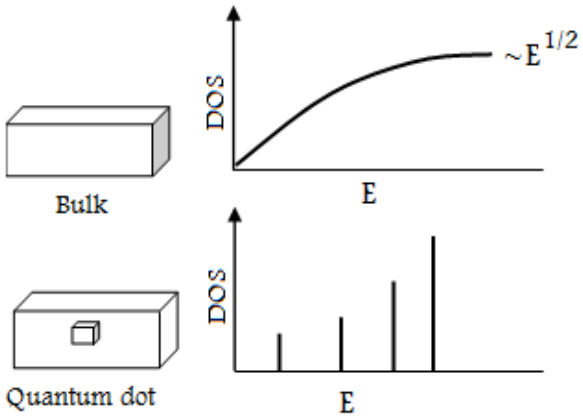

Figure 1.2: Schematic illustration of density of states for bulk and quantum dot materials.

illustrated in Fig.1.2

Another effect of quantum confinement is the freedom it gives to manipulate the "bandgap" of almost all materials at nano-level. The term "bandgap" has vague meaning at nanoscale since there is no well defined energy band structure, in general, that resemble macroscopic crystalline materials. In quantum dots bandgap represents the forbidden energy gap between the highest occupied and lowest unoccupied electronic states, and in this sense it has similar meaning with its bulk definition. This bandgap of quantum dots is very sensitive with physical dimension of confining potential at nanoscale. This very fascinating property, which can be exploited for various optical and electronic functions, is tackled extensively by range of approaches and by different researchers over the last two decades. In almost all approaches the bandgap of quantum dots are inversely related with its size in the following form

$$E_g^{Qd}(d) = E_g^{bulk} + A/d^{\alpha} \tag{1.2.1}$$

Where E_g is bulk energy gap, A and α are some positive constants that depend on

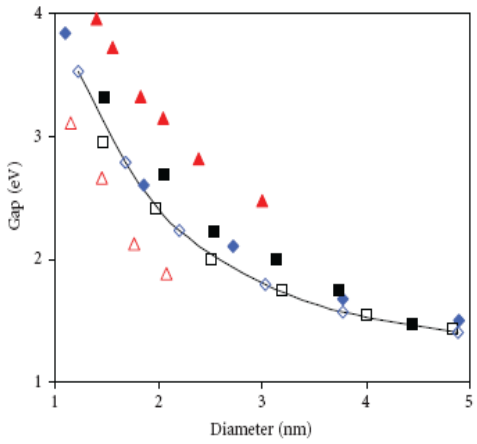

Figure 1.3: optical gap calculated by pseudo-potential (black and open squares), Tight-binding (blue, and open stars), and DFT (red and open triangles). All colored graphs are with out exciton correction, and none colored graphs are the corresponding bandgaps with exciton corrections[8].

the particular problem and the model employed. For example, using effective mass and infinitely deep quantum well approximations $\alpha = 2$, but the blue shift energy determined from experiments and better models doesn't follow A/d^2 law. Rather its dependence is , for instance, $\sim d^{-1.39}$[6]. Furthermore, both ab initio as well as semiemperical electronic structure calculations on Si cluster suggested values of α in the range 1.4-2 [7]. V.A. Belyakov et al. summarized the experimental data on the size dependence of the optical gap of silicon crystallites done by different workers and methods as shown in fig1.3 [8]. Later in chapter two, I have presented energy versus size relation, that are calculated based on finite potential well approximations.

Quantum confinement localizes the electronic states inside nc-Si in real space. Due to Heisenberg uncertainty relation ($\Delta x \Delta p \geq h$) the momentum distribution of the carriers spreads in momentum space, which in turn allows possibility of direct radiative transitions that gets stronger as we decrease the the size of the sample due

to overlap of momentum of electron and hole state which initially were separated by $\Delta k = 0.85(2\pi/a)$ in their bulk form. Hybertsen obtained strong contribution of direct radiative transition life time,inside quantum dot, near microsecond for cubic side near 2 nm, using effective mass and infinitely deep quantum well approximations[9]. The momentum spread of electronic state wave function also enhances the indirect phonon assisted transition to reach life time of order $\sim 10^{-5}$ near 2 nm diameter[8],[9]. Later in chapter 2 and 3, direct and phonon assisted transition rates are calculated based on finite potential well approximation.

Earlier studies on dependency of dielectric function of nc-Si was based on quantum confinement effect, but recent models are based on the breaking of polarizable bonds on the surface (surface effect) rather than the opening of band gap due to quantum confinement. In both cases, It is found that both real and imaginary parts of complex dielectric function reduce as the size of Si nanostructures decrease. The effect of this reduction on the optical response of nc-Si is matter of few units of order, but it strongly affects photon extraction efficiency due to the fact that photons are getting more gathered inside smaller dielectric constant material.

Apart from quantum confinement of carriers, reduction in size decrease the non-radiative transition rates by eliminating nanoradiative centers. This in turn has valuable effect on quantum efficiency of nanostructures. Quantum efficiency is the ratio of radiative recombination rates to total recombination rate. In general, It can be improved in two possible ways, either through increasing radiative recombination rates or decreasing nonradiative rates. In nanostructures, where there is considerable confinement of carriers, both of these improvements takes place. Quantum dots are either bright or dark depending on whether nonradiative centers are absent or

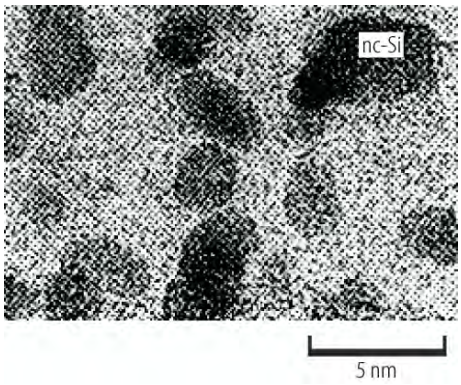

Figure 1.4: A typical photograph of an anodized nanocrystalline PS structure observed with transmission electron microscopy.

present. Luminescence efficiency of bright quantum dots is very high and that of dark quantum dots is very small, the overall distribution of bright and dark quantum dots in the ensemble determine the quantum efficiency of the material.

1.3 Luminescence from Oxidized Porous Si and Si Nanocrystallite inside SiO_2

Light emission from oxidized porous Si and nc-Si embedded in bulk SiO_2 matrix shares many similar features. The results obtained for one also applies to the other under some minor modifications and preconditions. In this paper we refer both of these systerms as nc-Si inside SiO_2. PL from PS is observable ranging from the ultraviolet[3] to infrared and it generally forms three bands named: blue, red and infrared. These three PL bands have peculiar characteristics and are caused by different mechanisms.

Blue PL band (400nm-500nm wave length): this part of PL is observed with lifetime of nanosecond order with exponential decaying rate. It is independent

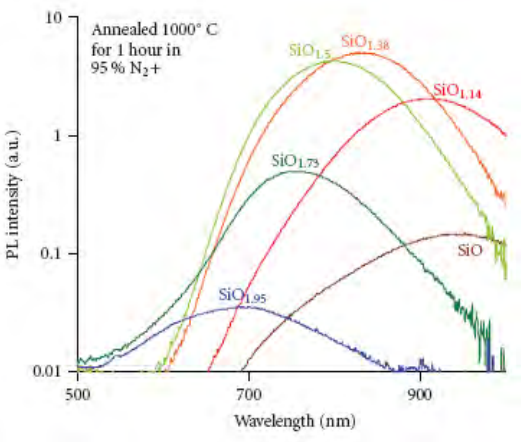

Figure 1.5: PL spectra of Silicon NCs in SiO_2. The size of nc-Si is controlled by amount of excess silicon. The smallest size is the one that is deficient with Si.

of both temperature, and excitation wavelength. However, quantum efficiency and reproducibility of PL is poor [10, 12, 13, 28].

Red PL band (560nm-860nm wave length): this attracts much attention because it is the only band that can be electrically excited. All types of porous silicon show red PL band provided porosity is sufficiently high. Its life time ranges from μs at room temperature to ms at 4.2 with PL decay of stretched exponential type. It has quantum efficiency of (5 percent) which is better than that of the blue PL band [2, 10, 11].

Infrared PL band (900nm to 2μm wave length): This band has broad spectrum and it can be observed at wavelengths greater than $2\mu m$. The radiative rates ranges from tens of nanoseconds to $10\mu s$. These times are generally faster than the decay of 'red' PL at the same temperature[10].

1.4 Luminescence Mechanism Models for Oxidized Silicon Nanostructures

Various many models are proposed to explain light emitting property of nc-Si embedded inside SiO_2 matrix and oxidized porous silicon, after pioneering report by canham[2] of efficient luminescence from porous silicon in (1990). However, there is still a debate in developing unified model that could explain the overall experimental records of luminescence from nc-Si. Models that are used widely for the understanding of light emission properties of nc-Si in SiO_2 are categorized under: Quantum confinement, surface state, Luminescence center and combination of these models.

Quantum confinement model: In quantum confinement model both photoexcitation and photoemission takes place inside nc-Si. The blue shift of PL peak in decreasing size is explained by the widening of the bandgap, and experimentally observed increment of radiative rates are attributed to strong momentum overlap between conduction band electron states and valence band hole states that comes as a result of quantum confinement. When the size of our sample is more and more reduced, electron's and hole's momentum gets more spread and their momentum distribution significantly overlap, particularly below 5 nm diameter size. The momentum overlap of carries makes it possible direct band to band recombination and enhances phonon assisted transitions from their bulk value ($\sim 10^{-3}s^{-1}$)[2, 8, 9]. Even though, the radiative lifetime calculated based on quantum confinement effect shows large improvement from that of bulk c-Si, it is in the order of μs for both zero phonon and phonon assisted transitions at smallest size even less than (2 nm). This relaxation rate is much lower than the decay rate of blue and infrared PL bands discussed earlier. The other important point is that the broadening of the bandgap below 2

nm determined from quantum confinement has sharp increase outside the range of any experimental and better model reports. Quantum confinement model, therefore, faces serious challenges in the size limit below 2 nm[2, 9]. By analyzing spectroscopic data from PS(porous Si), Kanemitsu et al in 1994 reported strong correlation between blue PL band and core region of PS, and red PL band with surface state at the interface and defects states inside SiO_2 [28]. There are also reports that support surface state model for red PL band [19]. However, the lifetime calculated by quantum confinement model is greater than (order of μs)even for quantum dot size less than 2nm. The calculated lifetime from quantum confinement corresponds to red PL band instead of blue band whose value is in nanosecond order. This is the point where the debate on luminescence mechanism starts and never ends till today. It is now believed that quantum confinement model works for slower decay rate transition (μs order) and calls other models for faster decaying rates[15, 16, 14].

"why radiative transitions that are reported to happen inside the nc-Si are not understood correctly by the quantum confinement model?" This is central question we raised in this paper and tried to address it based on different point of view. Before answering this question, it is good to see the kind of approximations incorporated in the quantum confinement model. Quantum confinement that has been studied and employed so far, for the case of nc-Si, involves crude approximation called infinitely deep quantum well and envelope wave function approximations which confines electron-hole pairs entirely inside nc-Si. The cause of this assumption is the band offset (3.2 eV and 4.6 eV for the electron and hole respectively) which occurs at the interface of nc-Si and SiO_2. These band offsets are assumed to be very large that the contribution of the wave function from the outside region is negligible[8, 9]. There

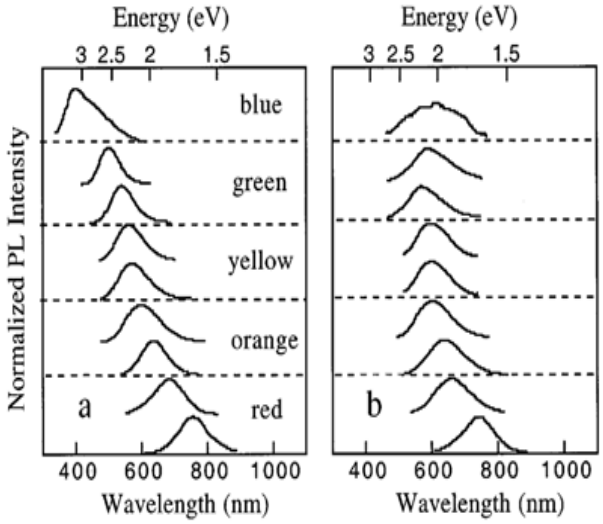

Figure 1.6: Room temperature PL spectra from PS samples with different porosities kept under Ar atmosphere (a) and after exposure to air (b)[17]

will be more discussion on this quantum confinement model in chapter two. Finally, It is worth remarking that, ***G.G Qin and G. Qin has reported approximately same value obtained from infinitely deep quantum well approximation by considering actual potential well, though their reference for their proof is their unpublished work[14].***

Surface state and Luminescence center model: Due to large surface to volume ration of nc-Si, like all other nanomatials, the effects of surface states and luminescence centers in the SiO_2 layer have strong impact on the light emission property observed. Both models considers photoexcitation inside nc-Si due to large band gap of SiO_2 and low density of defect states. The excited electrons and holes, instead of combining inside nc-Si as quantum confinement model predicts, they either be trapped by surface states within the bandgap and recombine at the interface of the

two material as surface state model says[19], or they will tunnel through the interface and recombine in luminescence centers, based on luminescence center model[15, 16]. These two models are very essential especially to explain why the PL peak from oxidized PS doesn't follow a blue shift estimated by quantum confinement model illustrated by fig.1.6. It is now believed that more that one type of PL mechanisms are needed to understand the over all PL characteristics of PS and nc-Si in SiO_2, where quantum confinement plays the dominant role for slow-band luminescence and surface states and luminescence center are for fast-band luminescence[15, 16]. However, this is in complete contradiction with the other group who claims surface and defect states within the bandgap are the main causes for red-PL band[28].

1.5 Objectives of the Paper

1.5.1 General Objective

The general objective of this research is to study phonon assisted and zero phonon radiative lifetimes of electron-hole pair which are excited and recombine inside nc-Si, on the basis of more realistic assumption of finite potential well and envelope wave approximations.

1.5.2 Specific Objectives

The specific objectives of this thesis are

- To provide brief review of the general debate on PL mechanisms of PS and nc-Si inside SiO_2.
- To provide results of radiative transition rate calculations for oxidized nc-Si, estimated based on infinitely deep potential well quantum confinement model.
- To calculate the energy bandgap broadening and momentum overlap factor of nc-Si in SiO_2 based on finite potential well and envelope wave function approximations.
- To calculate zero-phonon and phonon assisted radiative rates for oxidized nc-Si based on finite potential well quantum confinement model.
- Finally, to compare the results obtained by finite potential well approximation with that of infinitely deep quantum well approximation.

1.6 Thesis Organization

This thesis is organized into Six chapters. The first chapter provides brief introduction on the effects of quantum confinement on light emitting properties of materials and introduces the basics of optical properties of PS and nc-Si in SiO_2 with corresponding PL mechanisms. In the second chapter we discuss the general features of envelope function approximation and infinitely deep potential well quantum confinement model and its radiative rate estimations. The third chapter provides nc-Si

model based on finite potential well and envelope wave approximations and calculate energy bandgap broadening, momentum overlap factor as well as zero phonon direct radiative band to band recombination rate as function of size. The forth chapter will present calculations of phonon assisted raditive recombination rates inside nc-Si based on assumptions and approximations we developed in the third chapter. Chapter five is dedicated to presentation of results we found in chapter three and four as well as on comparison between infinitely deep and finite potential well results. Finally, summary and conclusion on the work of the paper is presented in chapter six.

Chapter 2

Infinitely Deep Potential Well Quantum Confinement Model

Computation of electronic spectra in pure Nanocrystals can be classified in to two. In the first class we have the numerical first-principles, empirical, and semi-empirical methods, such as density functional theory (DFT), pseudopotential (PP) method (or various combinations of PP and DFT), tight binding models etc. All these methods require considerable computational time, particularly when the nanocrystal size is made to be large. In the second class we find analytical methods like envelope function approximation that combine effective mass approximation and **K.P** method. This method allows to perform calculations without restrictions on cluster size. Additionally, this approach can be used to find the higher excited states of the nanocrystal.

2.1 Envelope Function Approximation

The development of envelope wave function for spherical quantum dot begins from bloch functions, and involves K.P method. In this section we present only some important features of envelope wave approximation that will be used in calculations

we encounter later. An electronic energy eigenstate $|\phi_{n\mathbf{k}}\rangle$ in bulk crystalline solid obeys the time-independent Schrödinger equation

$$[\frac{p^2}{2m_o} + U(\mathbf{r})]|\phi_{n\mathbf{k}}\rangle = \varepsilon_{n\mathbf{k}}|\phi_{n\mathbf{k}}\rangle \tag{2.1.1}$$

where m_o is mass of free electron, n is the band index, $\mathbf{k}$ is wave vector and $U(\mathbf{r}) = U(\mathbf{r}+\mathbf{R})$ for all $\mathbf{R}$ in Bravais lattice. Based on Bloch theorem, the solution of above differential equation is plane wave times a function with the periodicity of the Bravais lattice.

$$\langle\mathbf{r}|\phi_{n\mathbf{k}}\rangle = \exp(i\mathbf{k}\cdot\mathbf{r})\chi_{n\mathbf{k}}(r) \tag{2.1.2}$$

where $\chi_{n\mathbf{k}}(r) = \langle\mathbf{r}|n\mathbf{k}\rangle$, and it is the coordinate representation of lattice periodic part with Bravais lattice periodicity $\chi_{n\mathbf{k}}(\mathbf{r}+\mathbf{R}) = \chi_{n\mathbf{k}}(\mathbf{r})$. In quantum dots of interest in this and next chapters, the electronic energy eigenstate obeys the following time-independent Schrödinger equation

$$[\frac{p^2}{2m_o} + U(\mathbf{r}) + V_{cons}(r)]|\Phi_\lambda\rangle = \varepsilon_\lambda|\Phi_\lambda\rangle \tag{2.1.3}$$

where $V_{cons}(r)$ is confinement potential. Expanding quantum dot eigenstates in complete orthonormal basis set of Bloch eigenstates we get

$$|\Phi_\lambda\rangle = \sum_{n,\mathbf{k}} |\phi_{n\mathbf{k}}\rangle\langle\phi_{n\mathbf{k}}|\Phi_\lambda\rangle \tag{2.1.4}$$

and in coordinate representation it becomes

$$\langle\mathbf{r}|\Phi_\lambda\rangle = \sum_{n,\mathbf{k}} \exp(i\mathbf{k}\cdot\mathbf{r})\langle\mathbf{r}|\phi_{n\mathbf{k}}\rangle\langle\phi_{n\mathbf{k}}|\Phi_\lambda\rangle \tag{2.1.5}$$

Bloch functions are complete set at each $\mathbf{k}$, expanding the periodic part in terms of

the eigenstates at $\mathbf{k}$ of our choice say $\mathbf{k}_o$ we get

$$\langle \mathbf{r}|\Phi_\lambda\rangle = \sum_{m,n,\mathbf{k}} \exp(i\mathbf{k}\cdot\mathbf{r})\langle \mathbf{r}|m,\mathbf{k}_o\rangle\langle m,\mathbf{k}_o|\phi_{n\mathbf{k}}\rangle\langle\phi_{n\mathbf{k}}|\Phi_\lambda\rangle \tag{2.1.6}$$

$$= \sum_m [\sum_{\mathbf{k}} \exp(i\mathbf{k}\cdot\mathbf{r})F_{\lambda m\mathbf{k}}]\langle \mathbf{r}|m,\mathbf{k}_o\rangle \tag{2.1.7}$$

where

$$F_{\lambda m\mathbf{k}} = \sum_n \langle m,\mathbf{k}_o|\phi_{n\mathbf{k}}\rangle\langle\phi_{n\mathbf{k}}|\Phi_\lambda\rangle \tag{2.1.8}$$

again this can be written as

$$\langle \mathbf{r}|\Phi_\lambda\rangle = \sum_m F_{\lambda m}(R)\langle \mathbf{r}|m,\mathbf{k}_o\rangle \tag{2.1.9}$$

where

$$F_{\lambda m}(\mathbf{R}) = \sum_{\mathbf{k}} \exp(i\mathbf{k}\cdot\mathbf{r})F_{\lambda m\mathbf{k}} \tag{2.1.10}$$

The function $F_m(R)$ plays the role of envelope function as it varies very slowly compared to the central cell periodic Bloch part. The other beauty of envelop function is, it satisfies the following appropriately modified Schrödinger equation

$$[-\frac{\hbar^2\nabla^2}{2m_n^*} + V_{cons}(r)]F_{\lambda m}(\mathbf{R}) = \varepsilon_\lambda F_{\lambda m}(\mathbf{R}) \tag{2.1.11}$$

where m_n^* is effective mass of n^{th} band. Envelope functions are macroscopic approximations, they do not see fluctuations with in unit cells. They are used when the potential $V_{cons}(r)$ varies very slowly and assumed to be constant with in unit cell.

2.2 Infinitely Deep Potential Well Quantum Confinement Model

2.2.1 Wave Functions and Energy Levels

As we discussed in the introductory chapter, the quantum confinement model studied for oxidized nc-Si based on envelope function approximation sofar, use infinitely deep potential well to confine carriers inside nc-Si. As we pointed out, the origin of this assumption is large band offset between bulk c-Si and the surrounding SiO_2 matrix. under this potential well assumption the modified Schrödinger equation that will be solved for the envelope function of conduction and valence band states is

$$[\frac{-\hbar^2}{2m_d^*}\nabla^2 + V(r)]\Psi_d(\mathbf{r}) = E_d\Psi_d(\mathbf{r}) \tag{2.2.1}$$

where $V(\mathbf{r}) = 0$ inside and $V(\mathbf{r}) = \infty$ outside the nc-Si. As a result of this quantum confinement, the bulk conduction(c) and the valence(v) bands split into series of discrete energy levels (energy shells in spherical quantum dot). Solving schrödinger like differential equation for spherical quantum dot of radius R in general gives[20]

$$\Psi_{dnlm}(\mathbf{r}) = Y_{lm}(\theta,\phi)\frac{1}{R}(\frac{2}{r})^{\frac{1}{2}}\frac{J_{l+\frac{1}{2}}(k_{nl}r)}{J_{l+\frac{3}{2}}(k_{nl}R)}\chi_d(\mathbf{r}) \tag{2.2.2}$$

$$E_d = \pm\frac{E_g}{2} + \frac{\hbar^2 k_{nl}^2}{2m_d^*} \tag{2.2.3}$$

where $-l \leq m \leq l$; $l = 0, 1, 2, ...$; $n = 0, 1, 2, ...$; and

$$J_{l+\frac{1}{2}}(k_{nl}R) = 0 \tag{2.2.4}$$

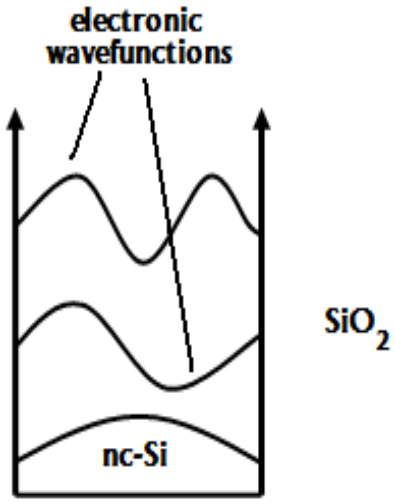

Figure 2.1: Schematic illustration of the lowest energy wave functions inside nc-Si from infinitely deep quantum well approximation.

here J_β is Bessel functions and Y_{lm} is normalized spherical harmonic functions. $\chi_d(\mathbf{r})$ are the central cell periodic parts of the bulk Bloch functions at the band edges, which are assumed to be unchanged. Where as for a cube quantum dot of width length L the electronic states takes the following form

$$\Psi_{dnlm}(\mathbf{r}) = (\frac{2}{L})^2 sin(\frac{n\pi}{L}x) sin(\frac{l\pi}{L}y) sin(\frac{z\pi}{L}z)\chi_d(\mathbf{r}) \tag{2.2.5}$$

$$E_{dnlm} = \pm\frac{E_g}{2} + \frac{\hbar^2\pi^2}{2m_d^* L^2}(n^2 + l^2 + m^2) \tag{2.2.6}$$

where $n, l, m = 1, 2, ...$ The energies are obtained from the requirement that the wave functions vanish at the corresponding quantum dot surfaces. The confinement of the carriers leads to blue shift of the electron and hole states. Moreover, the optical transition also become discrete like atomic transitions.

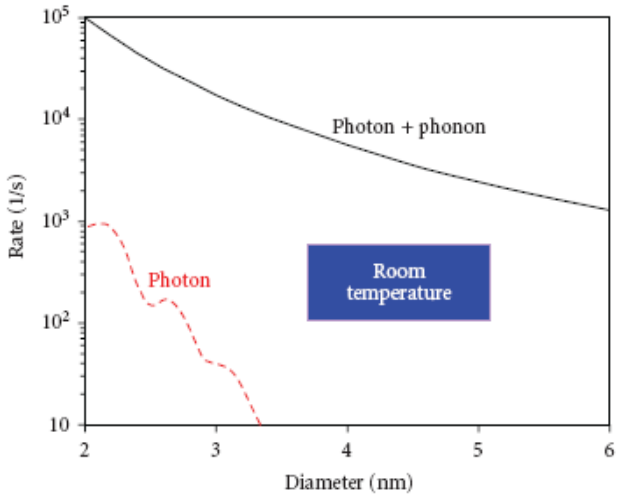

Figure 2.2: Recombination rates of no phonon and phonon-assisted radiative transitions between the ground electron and hole states in silicon NCs.

2.2.2 Radiative Recombination Rate

Based on infinitely deep potential well and envelope wave approximations, there are different reports of theoretical radiative recombination rate calculations inside nc-Si. In all reports the radiative recombination rate for nanocrystallite from 2-6nm in diameter do not exceed $10^5 s^{-1}$ and never less than $5 \times 10^2 s^{-1}$. However, the results may show slower or faster rate increment with in the specified range. Belyakove et al obtained $\frac{1}{R^3}$ and $\frac{1}{R^8}$ dependency on quantum dot radius, for phonon assisted and zero-phonon radiative recombination rates inside nc-Si respectively. His calculations are based on infinitely deep quantum well approximation. Even if zero-phonon (psedodirect) assisted radiative rate he calculated has none zero value below 3nm nanocystallinte diameter, it is very much small and radiative recombination processes are completely dominated by phonon assisted mechanisms in the size range above 2nm as summarized in fig.2.2[8]. Hybertsen also made theoretical calculations

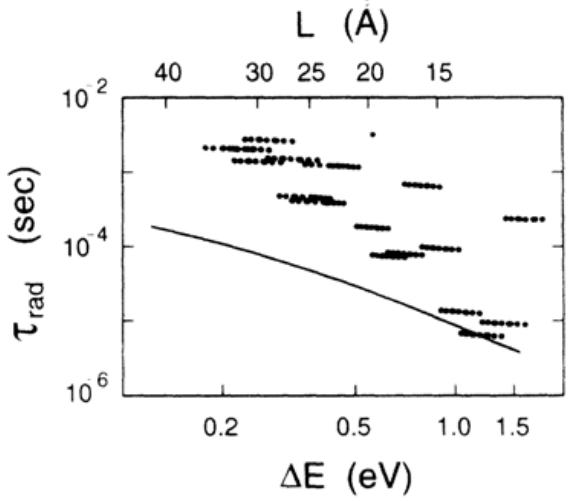

Figure 2.3: Radiative recombination time as function of blue shift of the photon energy from the bulk Si band edge. Zero-phonon transitions (dots): TO phonon-assisted transitions (line). This scatter plot shows the radiative lifetime for each member of an ensemble uniformly distributed around a cubic geometry. The top scale indicates the equivalent cube size.

on zero-phonon and phonon assisted radiative rates based on infinitely deep quantum well approximation[9]. He used cubic nanocrystallite of width L. The value he found for phonon assisted recombination rates are almost same in order with that of Belyakov et al calculations. However, Zero-phonon process, in his calculations, are strong and are comparable with phonon assisted process in the cubic size range of width length 1.5nm-2.0nm as illustrated in fig.2.3.

Chapter 3

Direct Radiative Transition Rate

3.1 Introduction

What makes analysis of luminescence data from oxidized P-Si and nc-Si embedded in SiO_2 difficult is the involvement of various radiative channels with interchanging dominance over the variation of size and particular preparation of the sample. Furthermore, most of photoluminescence data collected over the last 20 years is for ensemble of Si quantum dots, which makes the observed luminescence very broad as a result of inhomogeneous broadening. In such nc-Si ensemble, it is difficult to know which relaxation mechanism is dominant. Radiative transition rates vary with size for each mechanism with of course different degree. This variation is followed by an interchanging dominance of the radiative recombination mechanisms. Therefore, it is rational to see how each possible radiative channel behaves as we manipulate the dimension of our sample, before we draw any conclusion on general photoluminescence mechanism model that will explain every single feature of widely scattered data. In this paper, We only address two important radiative channels in Oxidized P-Si and nc-Si in $SiO2$, which are categorized under quantum confinement models.

3.2 Finite Potential Well Quantum Confinement Model

The improvement on luminescence property of Si nanocrystallites has three branches; the photoluminescence peak is blue shifted, the response time and quantum efficiency are highly improved. However, the whys of these very important results are still under strong debate. In most models developed so far, photoexcitation of carriers are assumed to occur inside quantum dot, since the surrounding material (SiO_2) is large bandgap (9 eV) dielectric material and the defects states on Si/SiO_2 interface has negligible contribution. Nevertheless, the proposed photoemission mechanisms are quite different from model to model with serious outcome difference even sometimes with contradiction. In quantum confinement model photoexcitation and photoemission occurs inside Si nanocrytallite. The blue shift of emission wavelength and corresponding lifetime are calculated based on simple particle in a box model. We improved this feature and instead of taking infinitely deep quantum well where electronic state wave functions are confined completely inside quantum dot, we consider finite quantum well with depth corresponding to band offset between nc-Si and surrounding material. Based on this consideration direct and indirect radiative transition rates are calculated for photoemission process that comes from electron and hole states inside nc-Si.

3.3 Wave Functions Used

The assumption of finite quantum well approximation modifies the wave functions that enters into Fermi Golden rule and calls more physical, mathematical and computational skills than that of infinitely deep quantum well approximation. Our nc-Si

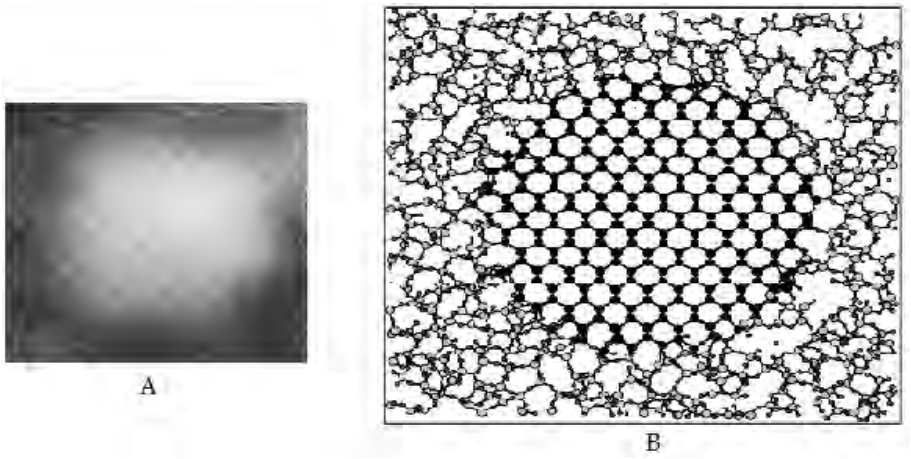

Figure 3.1: (a) Typical high resolution energy filtered TEM image of Si-nc, (b) Ball and stick model of nc-Si embedded in a-SiO_2. Dark sphere show Si atoms in the nano crystal, and Large (small) gray spheres denotes Si (O) atoms in the oxide, respectively [18]

is spherical quantum dot embedded in SiO_2 crystal. Using envelope wave approximation the envelope wave inside nc-Si are calculated. The anisotropic conduction band structure of c-Si is substituted by spherical band using the following modification on the effective mass of electron[22]

$$\frac{1}{m_e^*} = \frac{1}{3}(\frac{2}{m_e^\perp} + \frac{1}{m_e^\parallel}) \tag{3.3.1}$$

where m_e^*, $m_e^\perp$, and $m_e^\parallel$ are mean, perpendicular and parallel conduction-band effective masses. Since, we are only interested in the lowest energy transitions, we assume the valence band degeneracy is lifted due to quantum confinement effect and the electronic states considered in our work is heavy hole states.

Based on envelope wave approximation the envelope wave functions for electron and hole are obtained solving the following time independent Schrödinger equations

$$[\frac{-\hbar^2}{2m_d^*}\nabla^2 + V(r)]\varphi_d(\mathbf{r}) = E_d\varphi_d(\mathbf{r}) \tag{3.3.2}$$

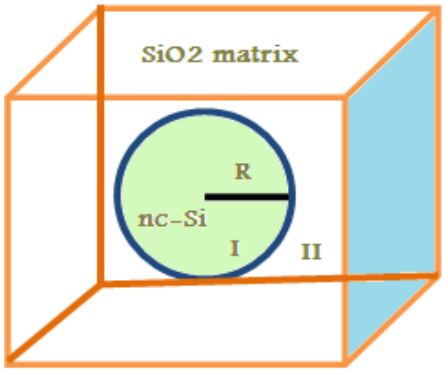

Figure 3.2: Spherical quantum dot model used for the derivations of electronic states wave functions inside nc-Si.

where $'d'$ is $'e'$ for electron and $'h'$ for hole. In region I, the value of the effective masses are the same as the value of c-Si; but in region two, the carriers are neither in conduction nor in valence band instead they are close to the fermi level. Hence, we apply mass discontinuity at the boundary and the masses of carriers in SiO_2 matrix are different from their vacuum value because they are in dielectric material. Many authors replace free electron mass as a first approximation in such circumstances[23]. $V(r)$ is taken to be zero in region I, and is equal to corresponding band offset between c-Si and SiO_2 in region II. Solving the differential equation in each region we get

In region I

$$\varphi_{di}(r) = Aj_l(k_{dl}r)Y_{lm}(\theta,\phi) + Bn_l(k_{dl}r)Y_{lm}(\theta,\phi) \tag{3.3.3}$$

where A and B are some constants, j_l, n_l, are spherical bessel functions of first and second kind respectively, Y_{lm} is spherical harmonic function, and

$$k_{dl} = \sqrt{\frac{2m_d^*}{\hbar^2}(E_{dl})}$$

In region II

$$\varphi_{do} = A'i_l(k'_{dl}r)Y_{lm}(\theta,\phi) + B'k''_l(k'_{dl}r)Y_{lm}(\theta,\phi) \tag{3.3.4}$$

where A' and B' are some constants, i_l, and k_l'' are modified spherical bessel functions of first and second kind, and

$$k'_{dl} = \sqrt{\frac{2m^*_{do}}{\hbar^2}(V_d - E_{dl})}$$

where m^*_{do} is effective masses of electron and hole out side nc-Si. To make our wave functions finite every where, we set $B = A' = 0$ as bessel function of second kind diverges at $r = 0$ and modified bessel function of first kind diverges at large r. Since our objective is to find the lowest energy transitions and energy gap, we consider only ground state wave functions in both regions. As a result the wave functions of interest reduces to the following form, putting l=0 in equation 3.3.3 and 3.3.4

In region I

$$\varphi_{di}(r) = \frac{A}{\sqrt{4\pi}}\frac{\sin(k_d r)}{k_d r} \tag{3.3.5}$$

In region II

$$\varphi_{do}(r) = \frac{B'}{\sqrt{4\pi}}\frac{\exp(k'_d r)}{k'_d r} \tag{3.3.6}$$

Wave functions must be continuous everywhere and integrable, so we apply the following continuity conditions at the interface $r = R$

$$\varphi_{di}(R) = \varphi_{do}(R) \tag{3.3.7}$$

$$\varphi'_{di}(R) = \varphi'_{d0}(R) \tag{3.3.8}$$

and normalizing the wave functions over real space we get

$$\varphi_{di}(r) = A_d\frac{\sin(k_d r)}{r} \tag{3.3.9}$$

$$\varphi_{do}(r) = B_d\frac{\exp(k'_d r)}{r} \tag{3.3.10}$$

where

$$A_d = \frac{\sqrt{k'_d}}{\sqrt{\pi[(\frac{k'_d}{k_d})(2k_dR - \sin(2k_dR)) - 2\sin^2(k_dR)]}} \tag{3.3.11}$$

$$B_d = \frac{\sqrt{k'_d}\sin(k_dR)\exp(k'_dR)}{\sqrt{\pi[(\frac{k'_d}{k_d})(2k_dR - \sin(2k_dR)) - 2\sin^2(k_dR)]}} \tag{3.3.12}$$

Moreover, we get the following transcendental equation that will let us determine the energies of electronic states

$$k_d \cot(k_dR) = -k'_d \tag{3.3.13}$$

solving this equation numerically, we are able to determine the energies of the electronic states for both electron and hole that make our wave functions continuous at the boundary and acceptable. The actual wave functions based on envelope wave function approximation are obtained including the central cell periodic parts of bulk c-Si. Because we allow the wave functions of the electronic states inside the nc-Si to spread into SiO_2, the use of the envelope function needs careful analysis outside the nc-Si. The energy levels of electron or hole outside nc-Si are close to neither the conduction band nor the valance band of SiO_2 matrix, rather they are close to the fermi level. This condition makes the expansion of the states in terms of band edge states to employe envelope wave approximation. In other words, the actual wave function expansion in terms of bulk Bloch functions inside SiO_2 involves valence band and conduction band states for both electron and hole states as they are close to the fermi level instead of either of the bands[23]. Therefore, the approximation we use for part of the wave function outside nc-Si is to take the the envelope wave function as a complete wave function similar to deeplevel wave function approximations used

in[23]. To summarize, we use the following wave functions for the calculations of direct and indirect radiative transition rates between electronic states inside nc-Si.

Inside nc-Si

$$\Psi_{di}(\mathbf{r}) = \varphi_{di}(r)\chi_d(\mathbf{r}) = A_d\frac{\sin(k_d r)}{r}\chi_d(\mathbf{r}) \tag{3.3.14}$$

Outside nc-Si

$$\Psi_{do}(\mathbf{r}) = \Psi_{do}(r) = \varphi_{do}(r) = B_d\frac{\exp(k'_d r)}{r} \tag{3.3.15}$$

where $\chi_d(r)$ is central cell periodic part of Bloach function.

3.4 Zero Phonon (Psedodirect) Recombination Rate

For Bulk c-Si lowest energy radiative recombination process completely involves phonon and it is a second order process. In nc-Si, however, there is definite probability for direct relaxation of electron from the conduction band to valence band with out involvement of phonons. This probability comes as a result of spread of momentum distribution of the carries when they are confined in real space. The degree of overlap depends sensitively on the size of the sample. For infinitely deep quantum well approximation Hybertsen[9] pointed out that below 1.5 nm width of cubic nc-Si, it is immaterial to talk about whether the material is direct or indirect.

We calculate spontaneous recombination rate R_{if} between initial electron state and final hole state without phonon involvement using Fermi Golden rule in the following form:

$$R_{if} = \frac{2\pi}{\hbar}\sum_{k_{ph},\sigma}|\langle h, n'|H'|e, n\rangle|^2\delta(E_g - \hbar\omega_\sigma(k_{ph})) \tag{3.4.1}$$

where $\omega_\sigma(k_{ph})$ stands for phonon frequency of wave vector k_{ph} and polarization σ, $\langle h, n'|$, and $|e, n\rangle$ are combined hole-final photon state and electron-initial photon

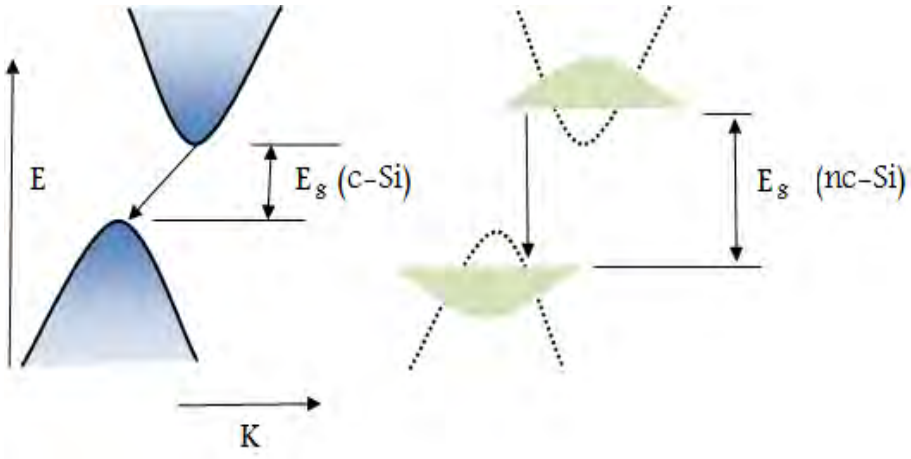

Figure 3.3: Schematic illustration of direct transition from conduction-band to valence-band, as a result of quantum confinement.

states respectively. The initial state corresponds to an electron-hole pair being in its ground state, and an ensemble of photons with occupation number $n_\sigma(k_{ph})$ that will be determined from Bose-Einstein statistics, and the final state is represented by increment of photon occupation number by one and annihilation of electron-hole pair. The operator H' represents the perturbation due to electromagnetic field that causes the scattering of electron and has the following form

$$H' = \frac{ie\hbar}{m_o}\mathbf{A}\cdot\nabla \tag{3.4.2}$$

here $\mathbf{A}$ stands for vector potential of electromagnetic radiation satisfying radiation gauge condition. Neglecting the momentum of photon, since it is very small compared to electron momentum and its contribution in breaking indirect nature of bulk c-Si band structure is negligible, the perturbing potential is given by

$$H' = -\frac{e}{m_o}\sqrt{\frac{\hbar}{2\omega_{ph}\epsilon V}}(b^\dagger + b)\mathbf{a}\cdot\mathbf{p} \tag{3.4.3}$$

where $b^\dagger$, b, $\mathbf{p}$ are creation, destruction and momentum operators. $\mathbf{a}$ is polarization unit vector and V is volume. Since our wave function of finite potential well

approximation is present in two media, the perturbing potential will not have same value over the effective dimension of the wave functions. We introduce variation of electron-electromagnetic interaction through dielectric permittivity. Therefore, we consider bulk silicon dielectric permittivity (ϵ_{si}) inside the quantum dot and bulk SiO_2 primitivity (ϵ_{so}) out side. Furthermore, due to size effect relative permittivity of nc-Si has reduced value from its bulk form. This effect is also introduced through dielectric function. In this work, we haven't used any correction on dielectric function that comes from the effect of reduced size. The matrix elements are calculated separately for photons and electronic states as they are in different spaces. For the photon states part, we will have the following result for photon emission where the final state increase by one photon number,

$$\langle n_{ph}+1|(b^{\dagger}+b)|n_{ph}\rangle = \sqrt{n_{ph}+1} \tag{3.4.4}$$

and the spontaneous radiative transition rate is calculated in the following manner

$$R_{if} = \frac{2\pi}{\hbar}(\frac{\hbar}{2\omega\epsilon_{si}})(\frac{e}{m_o})^2(n_{ph}+1)\sum_{k_{ph},\sigma}|\langle h|(\mathbf{a}.\mathbf{p})|e\rangle_{inside}+\langle h,|(\mathbf{a}.\mathbf{p})|e\rangle_{outside}|^2\delta(E_g-\hbar\omega_{\sigma}(k_{ph})) \tag{3.4.5}$$

where $n_{ph}=0$ to get rates for spontaneous emission. The matrix elements inside and outside nc-Si, based on envelope wave approximation are given by

$$\langle h|(\mathbf{a}.\mathbf{p})|e\rangle_{inside} = \langle \chi_h|(\mathbf{a}.\mathbf{p})|\chi_e\rangle \int_{r<R}\Psi^*_{hi}(\mathbf{r})\Psi_{ei}(\mathbf{r})d\mathbf{r} \tag{3.4.6}$$

$$\langle h|(\mathbf{a}.\mathbf{p})|e\rangle_{out} = \int_{r>R}\Psi^*_{ho}(\mathbf{r})(\mathbf{a}\cdot\mathbf{p})\Psi_{eo}(\mathbf{r})d\mathbf{r} \tag{3.4.7}$$

In bulk c-Si, this radiative transition rate is zero, because momentum selection rule doesn't allow direct transition between conduction and valence band edges states, i.e.,$\langle \chi_h|(\mathbf{a}.\mathbf{p})|\chi_e\rangle = 0$. However, as result of quantum confinement there is finite

probability for the conduction and valence band edge functions to have same momentum. This momentum overlap factor is the parameter that breaks indirect nature of bulk c-Si at nano-level. The overlap factor when there is momentum difference of k_0 is obtained by

$$\Upsilon(0, k_0; R) = \frac{\Psi_{h,k=o} * \Psi_{e,k=k_o}}{\int \Psi^*_{h,k=o} \Psi_{e,k=o} d\mathbf{k}} \tag{3.4.8}$$

where $\Psi_{h,k=o} * \Psi_{e,k=k_o}$ is convolution of Fourier transformed functions around $k = k_o$, and $k = 0$ for electron and hole respectively. k_o is the value of crystal momentum of conduction bandedge in first Brillouin zone. Using convolution and Perseval theorems[25] the momentum overlap factor reduces to

$$\Upsilon(0, k_0; R) = \frac{\int \Psi^*_h(r) \Psi_e(r) \exp(-i\hbar \mathbf{k}_o \cdot \mathbf{r}) d\mathbf{r}}{\int \Psi^*_h(r) \Psi_e(r) d\mathbf{r}} \tag{3.4.9}$$

Putting the the wave functions we developed in equations (3.3.14) and (3.3.15) earlier in radiative recombination rate and momentum overlap expressions we obtain the following pieces of calculations that will be put together later in radiative transition rate formula

$$\begin{aligned} \vartheta_{in} &= \int_{r<R} \Psi^*_{hi}(\mathbf{r}) \Psi_{ei}(\mathbf{r}) d\mathbf{r} \\ &= 2\pi A_h A_e [\frac{\sin((k_h - k_e)R)}{k_h - k_e} - \frac{\sin((k_h + k_e)R)}{k_h + k_e}] \end{aligned} \tag{3.4.10}$$

$$\begin{aligned} \vartheta_{ou} &= \int_{r>R} \Psi^*_{ho}(\mathbf{r}) \Psi_{eo}(\mathbf{r}) d\mathbf{r} \\ &= \frac{4\pi B_h B_e}{k'_h + k'_e} \exp(-(k'_h + k'_e)R) \end{aligned} \tag{3.4.11}$$

$$\zeta_{in} = \int_{r<R} \Psi^*_{hi}(r) \Psi_{ei}(r) \exp(-i\hbar \mathbf{k}_o \cdot \mathbf{r}) d\mathbf{r}$$

$$= \frac{4\pi A_h A_e}{k_0}[si((k_o+k_e-k_h)R)+si((k_o-k_e+k_h)R)-si((k_o+k_e+k_h)R)-si((k_o-k_e-k_h)R)] \tag{3.4.12}$$

where[25]

$$si(x) = -\int_x^\infty \frac{\sin(y)}{y}dy$$
$$\approx -\frac{\cos(x)}{x}\sum_{0<n<N}(-1)^n\frac{(2n)!}{x^{2n}} - \frac{\sin(x)}{x}\sum_{0<n<N}(-1)^n\frac{(2n+1)!}{x^{2n}} \tag{3.4.13}$$

$$\zeta_{ou} = \int_{r>R}\Psi^*_{h0}(r)\Psi_{eo}(r)\exp(-i\hbar\mathbf{k}_o\cdot\mathbf{r})d\mathbf{r}$$
$$= \frac{4\pi B_h B_e}{k_o}I(k_oR) \tag{3.4.14}$$

where (self developed series)

$$I(k_oR) = \int_R^\infty \frac{\exp(-(k'_h+k'_e)r)\sin(k_or)}{r}d\mathbf{r}$$
$$= \exp(-mx)[\sin(x)\sum_{n=1}^\infty\frac{(-1)^n}{(mx)^n}\sum_{s=0}^\infty\frac{(-1)^{s+1}(n+(2s-1))!}{(2s)!m^{2s}} - \cos(x)\sum_{n=1}^\infty\frac{(-1)^n}{(mx)^n}\sum_{s=0}^\infty\frac{(-1)^{s+1}(n+2s)!}{(2s+1)!m^{2s+1}}] \tag{3.4.15}$$

here m and x stands for $\frac{k'_h+k'_e}{k_o}$ and k_oR respectively. The momentum matrix outside nc-Si has zero value, i.e.

$$\langle h|(\mathbf{a}.\mathbf{p})|e\rangle_{out} = 0 \tag{3.4.16}$$

this comes as a result of same parity of wave functions outside the nc-Si. Using the above calculated values and considering approximately same value for $\langle h,\mathbf{k}|(\mathbf{a}\cdot\mathbf{p})|e,\mathbf{k}\rangle = P_{cv}$ independent of $\mathbf{k}$, where the value of P_{cv} is taken from experimental value, the spontaneous zero-phonon radiative recombination rate will have the following form

$$R_{eh} = \frac{2\pi}{\hbar}(\frac{\hbar}{2\omega\epsilon_{si}})(\frac{e}{m_o})^2\sum_{k_{ph},\sigma}|\Upsilon(0,k_o;R)\vartheta_{in}P_{cv}|^2\delta(E_g-\hbar\omega_\sigma(k_{ph})) \tag{3.4.17}$$

this equation is further simplified by replacing the sum over possible photon wave vector and polarization by the density of the photon states. The total photon density of states is given by

$$\rho(\hbar\omega) = \frac{\omega^2}{\pi^2 \hbar v^3} \tag{3.4.18}$$

where v is the speed of light in the sample. Using this value for photon density, and replacing E_p for $2|P_{cv}|^2/m_o$, equation (2.4.17) is further simplified to

$$R_{eh} = \frac{2\omega\sqrt{\epsilon_{si}}}{\pi\hbar\epsilon_o c^3}\frac{e^2}{m_o} E_p \Upsilon^2(0, k_e; R)\vartheta_{in}^2 \tag{3.4.19}$$

where $\hbar\omega = E_g(nc - Si)$ and using the results we found in equation (3.4.10), (3.4.11), (3.4.12) and (3.4.14) the momentum overlap function, in the above formula, is given by

$$\Upsilon(0, k_e; R) = \frac{\zeta_{in} + \zeta_{ou}}{\vartheta_{in} + \vartheta_{ou}} \tag{3.4.20}$$

Chapter 4

Phonon Assisted Relaxation of Carriers inside Si Nanocrystallite

4.1 Introduction

Phonon assisted transitions are also modified due to finite size effects. Momentum selection rule which peaks only single wave vector and its neighborhood in bulk Si is significantly relaxed when we substantially confine the carrier states. In another word, light emission from bulk c-Si are completely phonon mediated due to momentum selection rule. Furthermore, all phonon modes are not participating in the light emission process. Only phonons of wave vector $k_0 = 0.85(\frac{2\pi}{a})$ and its neighborhood are required for intervalley phonon scattering purpose to satisfy conservation of momentum. This highly restricted phonon wave vector requirement is significantly relaxed when electronic states are substantially confined.

The other effect of quantum confinement on phonon related processes is that, all bulk phonon modes are not present at nanostructures. Phonon modes are quantized in the same way electronic states in infinitely deep quantum well approximation are quantized. The phonon modes of one material does not propagate in to the other

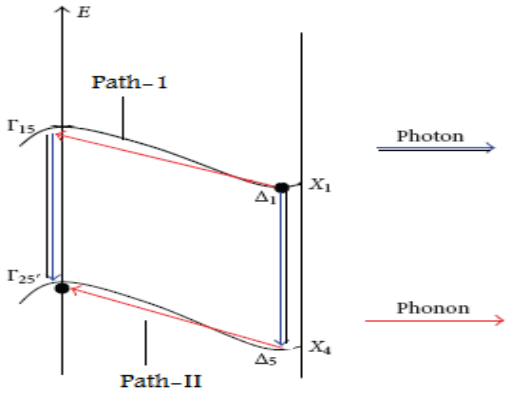

Figure 4.1: Schematic representation of the c-Si band structure with phonon-assisted radiative transition from the conduction band minimum to the valence-band maximum indicated by arrows.

material as phonon dispersion relation of one material is different from the other. Moreover, at the interface of the two materials, there is large amplitude vibrations whose effects are very significant to any process that participate phonons at nanolevel. Currently, phonon mediated processes in nanostructures are one of active area of research and calls advanced physical, mathematical, and computational skills[26]. In this paper, We present calculations of phonon assisted light emission process between electronic states present in nc-Si across the bandgap. The effect of quantization of phonon modes and surface large amplitude modes in optical region are approximated by scattering process where the phonon's interaction potential is bulk like and electrons and holes are described by the wave functions we developed in chapter two [27].

4.2 Phonon Assisted Relaxation Calculation in nc-Si

Typical processes in the interband transition are shown in fig.3.1. The process is second order in which the electron is first scattered by a phonon (path-I) to Γ_{15} conserving momentum and then scattered to the valence band by a photon. Similarly, in the other path transition, electron is first scattered by a photon then by a phonon. In these two processes energy is not conserved, since the process is virtual and the time-energy uncertainty ensures that there is no energy conservation requirement. The overall process, however, does conserve energy. The other fascinating story in these process is the interference between the oscillator strength for path-1 and for path-2. The oscillator strengthes for path-1 and path-2 may interfere constructively or destructively depending on particular phonon branch[22]. The scattering rate is again calculated based on Fermi golden rule except that the matrix element is second order

$$
\begin{aligned}
R_{ind} = \frac{2\pi}{\hbar}\sum_{\hbar\omega}\sum_{\sigma,q}|\frac{\langle v,0|H'|q,c\rangle\langle c,q|H^{\sigma}_{pn}|k_o,c\rangle}{E_{cq}-E_{c,k_o}-\hbar\omega_{\sigma q}} \\
+\frac{\langle v,0|H^{\sigma}_{pn}|k_o-q,v\rangle\langle v,k_o-q|H'|k_o,c\rangle}{E_{vq}-E_{v,k_o}-\hbar\omega_{\sigma q}}|^2\delta(E_g(nc-Si)-\hbar\omega-\hbar\omega_{\sigma q}) \\
+\frac{2\pi}{\hbar}\sum_{\hbar\omega}\sum_{\sigma,q}|\frac{\langle v,0|H'|q,c\rangle\langle c,q|H^{\sigma}_{pn}|k_o,c\rangle}{E_{cq}-E_{c,k_o}+\hbar\omega_{\sigma q}} \\
+\frac{\langle v,0|H^{\sigma}_{pn}|k_o-q,v\rangle\langle v,k_o-q|H'|k_o,c\rangle}{E_{vq}-E_{v,k_o}+\hbar\omega_{\sigma q}}|^2\delta(E_g(nc-Si)-\hbar\omega+\hbar\omega_{\sigma q}) \qquad (4.2.1)
\end{aligned}
$$

where the first sum is over possible photon states as used in previous chapter, the second sum is over all phonon branches (σ), and the third inner sum is over all

possible intermediate virtual states. $\omega_{\sigma q}$ signifies the frequency of phonon mode of wave vector q, and branch σ. H' and H^{σ}_{pn} represents electromagnetic and phonon perturbing potentials. The first term is due to emission of phonon and the second term is due to absorption of phonon obtained just by replacing $(-\hbar\omega_{\sigma q})$ by $(\hbar\omega_{\sigma q})$ everywhere it appears. k_o is the crystal momentum of bulk c-Si at Δ point. Here we must make it clear how this equation is used in our fundamental assumption of finite potential well approximation. In finite potential well approximation, the wave functions of electronic states crosses the interface and enters in to another material that have completely different phonon dispersion. The phonon matrix elements due to the wave functions outside nc-Si is not zero unlike momentum matrix elements. Therefore, to get better results, matrix elements from outside phonon perturbation must be included. However, in this paper, only phonon scattering due to inside phonon perturbation are considered as a matter of fact majority of the scattering are assumed to happen inside the nc-Si. Therefore, our crude assumption looks like this, phonon perturbations are $'on'$ inside nc-Si and $'off'$ out side/in SiO_2 matrix. Having these simplifying assumption equation 3.2.1 is cracked step by step in the following manner for nc-Si.

The momentum overlap factor: if we were applying equation 4.2.1 to bulk c-Si, the sum over q is zero except at one point $q = k_o$. Nevertheless, as a result of quantum confinement each term has none zero contribution to the total scattering rate. Following same procedure we developed in chapter two, the overlap factor is given by

$$\Upsilon(0, q; R) = \frac{\int \Psi^*_h(r)\Psi_e(r)\exp(-i\hbar\mathbf{q}\cdot\mathbf{r})d\mathbf{r}}{\int \Psi^*_h(r)\Psi_e(r)d\mathbf{r}} \tag{4.2.2}$$

Photon-electron interaction matrix element: the matrix element that contains electron and photon interaction will have none-zero value at each wave vector q due to momentum overlap factor, given by equation (4.2.2). The matrix element will be in the following form based on the facts we discussed in the previous chapter.

$$\langle v, 0|H'|q, c\rangle = \langle v, k_o - q|H'|k_o, c\rangle \tag{4.2.3}$$

$$= \sqrt{\frac{h}{2\omega\epsilon_{si}}}\frac{e}{m_o}\Upsilon(0, q; R)\vartheta_{in}P_{cv} \tag{4.2.4}$$

Phonon-electron/hole interaction matrix element: we initially pointed out that electron-phonon interactions considered are those that are inside the nc-Si. We have used experimentally determined electron-phonon and hole-phonon interaction matrix elements of indirect transitions in bulk c-Si after the following modifications.

$$\langle c, q|H^{\sigma}_{pn}|k_o, c\rangle = \frac{c_e S_{e-pn-\sigma}\sqrt{n_\sigma + \frac{1}{2} \pm \frac{1}{2}}}{\sqrt{N}} \tag{4.2.5}$$

$$\langle v, 0|H^{\sigma}_{pn}|k_o - q, v\rangle = \frac{c_h S_{h-pn-\sigma}\sqrt{n_\sigma + \frac{1}{2} \pm \frac{1}{2}}}{\sqrt{N}} \tag{4.2.6}$$

where $S_{e-pn-\sigma}$ and $S_{h-pn-\sigma}$ are electron-phonon (e-pn) and hole-phonon (h-pn) interaction matrix elements calculated for indirect transitions in bulk c-Si[22] for each

phonon branch σ. N is number of unit cells, n_σ is the occupation number of phonons at room temperature for each phonon branch σ. $+$ sign is used for phonon emission and $-$ sign for phonon absorption. c_d is calculated putting $'e'$ for electron and $'h'$ for hole in place of d in the following equation.

$$c_d = \int_{r<R} \varphi_{di}^2(r) d\mathbf{r} = \frac{1}{1 + \frac{k_d}{k'_d} \frac{2\sin^2(k_d R)}{2k_d R - \sin(2k_d R)}} \tag{4.2.7}$$

Putting values of momentum overlap factor equation (4.2.2), photon equation (4.2.3) and phonon matrix elements equation (4.2.4) and (4.2.5) in equation (4.2.1) we get the following result

$$\begin{aligned} R_{ind} = \frac{2\pi}{\hbar} \frac{\hbar}{2\omega\epsilon_{si}} (\frac{e}{m_o})^2 (\frac{1}{N}) \vartheta_{in}^2 P_{cv}^2 \{ & \sum_{\hbar\omega} \sum_{q} |\Upsilon(0,q;R)|^2 \sum_{\sigma} |\frac{c_e S_{e-pn-\sigma}}{E_{cq} - E_{c,k_o} - \hbar\omega_{\sigma q}} \\ & + \frac{c_h S_{h-pn-\sigma}}{E_{vq} - E_{v,k_o} - \hbar\omega_{\sigma q}}|^2 (n_\sigma + 1) \delta(E_g(nc-Si) - \hbar\omega - \hbar\omega_{\sigma q}) \\ & + \sum_{\hbar\omega} \sum_{q} |\Upsilon(0,q;R)|^2 \sum_{\sigma} |\frac{c_e S_{e-pn-\sigma}}{E_{cq} - E_{c,k_o} + \hbar\omega_{\sigma q}} \\ & + \frac{c_h S_{h-pn-\sigma}}{E_{vq} - E_{v,k_o} + \hbar\omega_{\sigma q}}|^2 n_\sigma \delta(E_g(nc-Si) - \hbar\omega + \hbar\omega_{\sigma q}) \} \end{aligned} \tag{4.2.8}$$

Neglecting phonon energy $\hbar\omega_{\sigma q}$ in the denominators and dirac delta argument because it is relatively small, and taking the energy arguments to be constant over the range of q as the dominant contribution comes from a restricted region near $q = k_o$; as well as, replacing the sum over photon states ($\hbar\omega$) by the density of photon states $\rho(\hbar\omega)$ stated in equation (3.4.18) the above equation further simplified into the form of

$$R_{ind} = \frac{2\pi}{\hbar}\frac{\hbar}{2\omega\epsilon_{si}}(\frac{e}{m_o})^2(\frac{1}{N})\vartheta_{in}^2 P_{cv}^2 \rho(\hbar\omega)\sum_q |\Upsilon(0,q;R)|^2$$
$$\times\sum_\sigma (2n_\sigma+1)|\frac{c_e S_{e-pn-\sigma}}{E_{c\Gamma}-E_{c,\Delta}}+\frac{c_h S_{h-pn-\sigma}}{E_{v\Gamma}-E_{v\Delta}}|^2 \tag{4.2.9}$$

The term that contains the overlap factor is calculated in the following way, using equation (3.4.10), (3.4.11) and (4.2.2)

$$\sum_{\mathbf{q}} |\Upsilon(0,\mathbf{q};R)|^2 = \frac{V}{(2\pi)^2}\int |\Upsilon(0,q;R)|^2 d\mathbf{q}$$
$$= \frac{V}{(2\pi)^2}(\frac{1}{(\vartheta_{in}+\vartheta_{ou})^2})[\int_{r<R}\varphi_{ei}^2\varphi_{hi}^2 d\mathbf{r}+\int_{r>R}\varphi_{eo}^2\varphi_{ho}^2 d\mathbf{r}]$$
$$= \frac{V}{(2\pi)^2}(\frac{1}{(\vartheta_{in}+\vartheta_{ou})^2})U(R) \tag{4.2.10}$$

where V is the volume of nc-Si and $U(R)$ is given by

$$U(R) = 4\pi A_e^2 A_h^2\int_{r<R}\frac{\sin^2(k_e r)\sin^2(k_h r)}{r^2}dr$$
$$+\int_{r>R}\frac{\exp(-2(k_h'+k_e'))}{r^2}dr$$
$$= 4\pi A_e^2 A_h^2[N(R)+\frac{\exp(-2(k_h'+k_e')}{R}-2(k_h'+k_e')Ei(-2(k_h'+k_e'))] \tag{4.2.11}$$

here $N(R)$, and $Ei(x)$ are in the following forms

$$Ei(x) \simeq \int_x^\infty \frac{\exp(-x)}{x} dx = \exp(-x) \sum_{0<n<N} \frac{(-1)^n n!}{x^{n+1}} \tag{4.2.12}$$

$$N(R) = \int_R^\infty \frac{\sin^2(k_e r)\sin^2(k_h r)}{r^2} dr$$
$$= \frac{k_e}{4} Gi(2k_e R) + \frac{k_h}{2} Gi(2k_h) - \frac{(k_e - k_h)}{4} Gi(2(k_e - k_h))$$
$$- \frac{(k_e + k_h)}{4} Gi(2(k_e + k_h)) - \frac{1}{R}\sin^2(k_e R)\sin^2(k_h R) \tag{4.2.13}$$

where

$$Gi(x) = \frac{\pi}{2} + Si(x)$$

Using the value of photon density of states stated in equation (3.4.18), and replacing the value of the term that contains the overlap factor we get

$$R_{ind} = \frac{e^2 \omega E_p \sqrt{\epsilon_{si}} V_{cell}}{4\hbar\pi^4 c^3 m_o \epsilon_o} \frac{\vartheta_{in}^2}{(\vartheta_{in} + \vartheta_{ou})^2} U(R) \sum_\sigma (2n_\sigma + 1) \left| \frac{c_e S_{e-pn-\sigma}}{E_{c\Gamma} - E_{c,\Delta}} + \frac{c_h S_{h-pn-\sigma}}{E_{v\Gamma} - E_{v\Delta}} \right|^2 \tag{4.2.14}$$

where V_{cell} is volume of unit cell, c is speed of light, ϵ_o is vacuum permittivity and m_o is rest mass of electron in free space.

Chapter 5

Results and Discussions

This chapter is dedicated to presentation of results from our finite potential well approximation for bandgap energy (equation 3.3.13), phonon assisted (equation 4.1.15) and zero-phonon (equation 3.4.19) radiative transition rates with in nc-Si. Furthermore, it provides brief comparison between finite and infinitely deep potential well results. The chapter is concluded by making general remarks on the exciton and dielectric constant effects on the results we found.

5.1 Bandgap Energy

Our assumption of considering finite quantum well approximation bring us valuable modifications stating from improving the broadening of bandgap energy predicted by infinitely deep quantum confinement model. Solving computationally (Appendix) the transcendental equation we get from continuity boundary conditions as well as using effective mass discontinuity approximation at the interface in equation (3.3.13), we obtain energy bandgap widening as function of nc-Si size summarized by figure 5.1 and table 5.1. The effective masses used in our calculations are: mean effective mass of electron $m_e^* = 0.26m_0$ and effective mass of heavy hole $m_h^* = 0.54m_o$ where

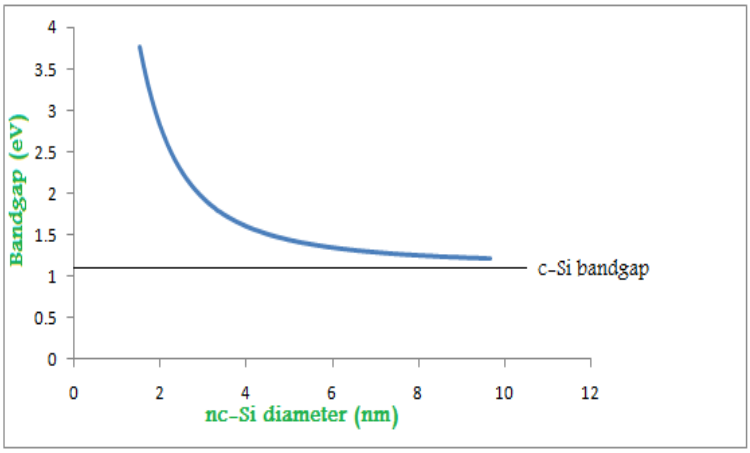

Figure 5.1: Bandgap energy vs nc-Si quantum dot size obtained by finite potential well approximation.

m_o is rest mass of electron in free space inside nc-Si. Out side nc-Si, both masses of electron and hole are taken to be equal to m_o.

From the results illustrated in the fig.5.1, 5.2, it is clear that the blue-shift from finite quantum well approximation doesn't follow exact $\frac{1}{R^2}$ similar to infinitely deep potential well estimates, rather it follows $\frac{1}{R^b}$ with $b < 2$ closer to values predicted by other models fig 1.3. When we compare between finite and infinitely deep potential well approximations summarized by Table 5.1, fig. 5.2,5.3; the difference between the two quantum confinement models is more pronounced at smaller size particularly 2-3nm. Infinite potential well energies blows up below 2nm and they can not be used for calculations since the energies below 2 nm is comparable with band offset at the interface. This drawback of infinitely deep quantum well model is significantly improved by finite potential well approximation. Finite potential energies can be used for calculations with size ranges 1-2nm.

nc-Si diameter (nm)	Bandgap energy (eV) (Infinitely deep well appr.)	Bandgap energy (eV) (Finite well appr.)
1.0	14.7	5.8
1.2	10.6	4.9
1.33	8.8	4.4
1.46	7.4	4.0
1.60	6.4	3.6
1.73	5.7	3.3
2.0	4.5	2.8
2.4	3.5	2.4
3.0	2.6	1.94
4.0	2.0	1.6
7.0	1.4	1.3
9.6	1.26	1.21

Table 5.1: Comparison of bandgap energy between infinitely deep and finite potential approximations at different nc-Si diameter.

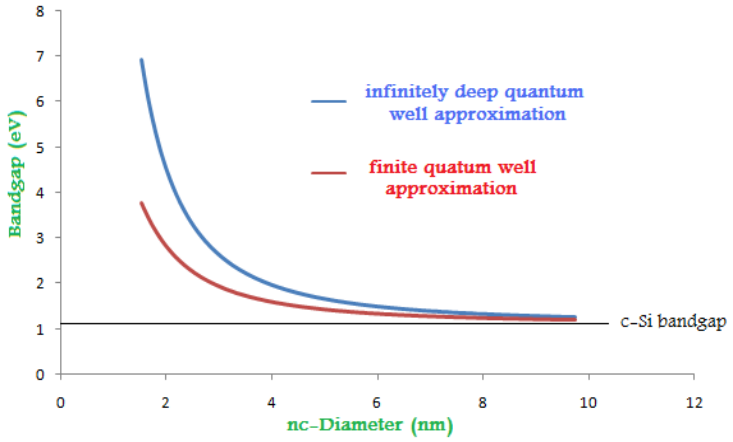

Figure 5.2: Bandgap energy vs nc-Si quantum dot size from infinitely deep quantum well approximation (blue), and finite quantum well approximations (red). The graphs are drawn on same scale.

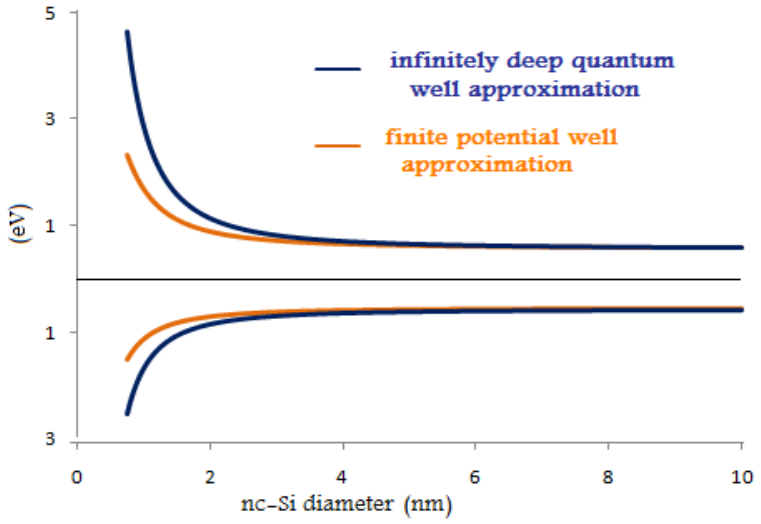

Figure 5.3: Electron and hole band edge energies as a function of size for infinitely deep quantum well potential approximation (blue), and finite potential approximation (red). The graphs are drawn on same scale.

5.2 Zero-Phonon (Psedodirect) Radiative Recombination Rate/Lifetime

To calculate spontaneous radiative recombination rate and radiative life time for zero phonon process, we use the value of $E_p = 4eV$ determined from **k.p** method for bulk c-Si and the energies we have calculated at each R from finite potential approximation in equation (3.3.13). It is good to see first, how the momentum overlap factor behaves with size as it is the cause of most luminescence property changes at nano-level. The momentum overlap factor (equation 3.4.20) is calculated separately and illustrated in fig.5.4. Below 2.5 nm diameter it is considerable and encourages direct recombination. Particularly between 1nm-1.25nm it is close to unity and results very strong direct recombination rate. Zero phonon spontaneous recombination rate (equation

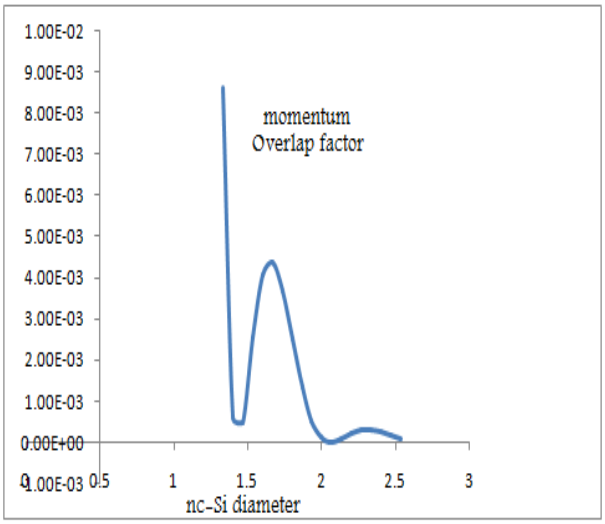

Figure 5.4: Momentum overlap factor (Υ^2) as function of size between 1.333nm, and 2.533nm.

3.4.19) is calculated and the results summarized by fig.5.5 and table 5.2 are generated. Due to quantum confinement effect, direct band to band transitions starts to contribute to luminescence property of nc-Si at size below 3nm. Particularly for nc-Si between 2.5nm the calculated values have significant contribution as one radiative relaxation mechanism. The average lifetimes obtained are summarized by the table 2.1. As clearly illustrated in fig.5.5 and table5.2, the lifetime of direct band to band transitions gets stronger as we confine the carriers more and more. Particularly, in the region of 1.0-2.0 nm, the direct relaxation is very fast in the order of nanosecond. Which suggest the possibility of blue emission from crystalline core.

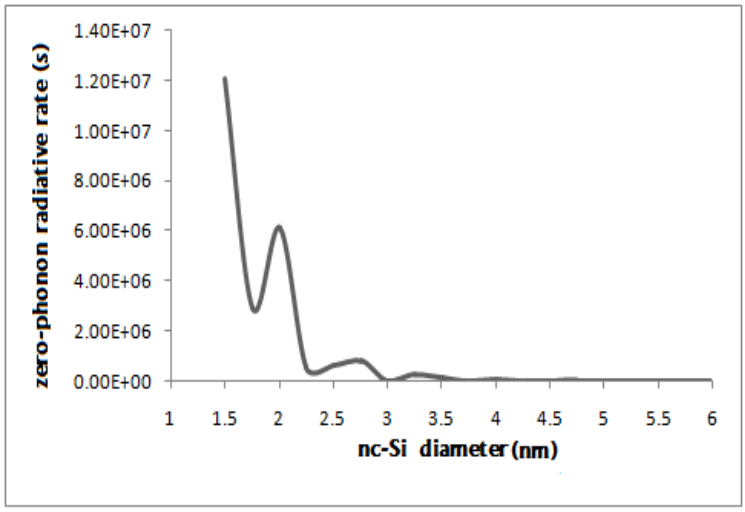

Figure 5.5: Spontaneous radiative band to band recombination rate with zero phonon involvement

nc-Si, diameter (nm)	Radiative recombination rate (s^{-1})	lifetime(s)
1-1.3	$\sim 10^{9}$	$\sim 10^{-10} - 10^{-9}$
$1.3 - 2.0$	$\sim 10^{7} - 10^{8}$	$\sim 10^{-8}$
$2.0 - 3.12$	$\sim 10^{5} - 10^{6}$	$\sim 10^{-7} - 10^{-6}$
$3.12 - 3.8$	$\sim 10^{4}$	$\sim 10^{-5}$
above 3.8	$< 10^{4}$	$> 10^{-5}$

Table 5.2: Relaxation rate and lifetime for zero phonon band to band transitions for different ranges nc-Si size.

5.3 Phonon Assisted Radiative Recombination Rate

Phonon assisted de-excitation of carriers inside nc-Si is calculated at room temperature. The electron and hole matrix elements of transverse optical phonon(TO) interfere constructively and they have strong relative intensities compared to other phonon branches. In our calculations we use only transverse and longitudinal optical (LO)modes. We assumed the relative intensities of bulk c-Si values (1.0, 0.15, 0.03)[22] for TO, LA, and TA (transverse acoustic) phonons respectively are maintained in our nc-Si sample. Neglecting TA modes as they contribute very small to the total scattering rate, energy values of 57.5 meV, and 55.3 meV are used for TO and LO modes respectively. We used experimentally obtained values $S_{e-pn-TO} = 15.3 \times 10^{-3} Ry$ and $S_{h-pn-To} = -18.7 \times 10^{-3} Ry$[22] for TO phonon in our calculation. And the matrix elements for Lo phonon is calculated using relative intensity given above. The occupation number for TO and LO phonons at room temperature and at the specified energies are 0.12 and 0.14 respectively when they are calculated using Bose-Einstein distribution ($\frac{1}{\exp(\frac{\hbar\omega}{k_B T})-1}$). 2.3 eV and -3.5 eV values are used for $(E_{c\Gamma} - E_{c\Delta})$ and $(E_{v\Gamma} - E_{v\Delta})$ respectively. Finally putting these values in equation (4.2.15), we are able to calculate phonon assisted spontaneous radiative recombination rate for nc-Si inside SiO_2 using finite well approximation. The values calculated by finite potential well consideration are not significantly different from that of infinitely deep quantum well approximations unlike zero-phonon radiative transition rate. figure 5.6, and Table 5.3 illustrate radiative relaxation rate as a function of size inside nc-Si. The radiative transition rates calculated are contributions that comes from quantum confinement effect and they will go to zero instead of going to the bulk c-Si indirect transition rates.

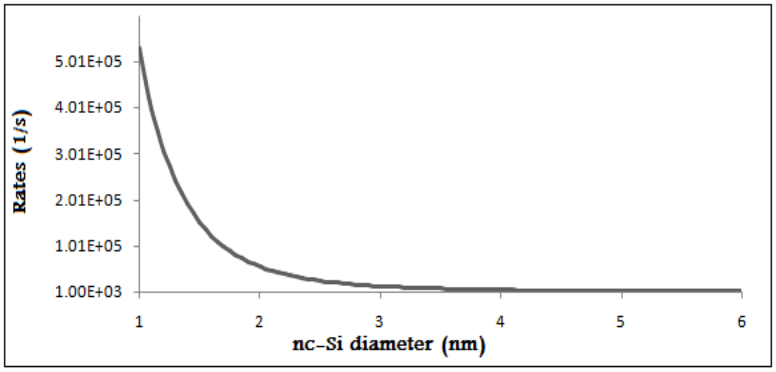

Figure 5.6: Phonon assisted relaxation rate, calculated based on finite potential well approximation Vs diameter of nc-Si in side SiO_2

nc-Si diameter (nm) (nm)	Phonon assisted relaxation rate(s^{-1})	phonon assisted relaxation rate(s)
1-1.6	$\sim 10^5$	$\sim 10^{-6}$
1.6-3.2	$\sim 10^4$	$\sim 10^{-5}$
3.2-6.3	$\sim 10^3$	$\sim 10^{-4}$
6.4-13	$\sim 10^2$	$\sim 10^{-3}$
above 13	$< 10^2$	$> 10^{-3}$

Table 5.3: Phonon assisted relaxation rate and lifetime in several ranges of nc-Si size, calculated based on finite potential well approximation.

5.4 Comparison Between Finite and Infinitely Deep Potential Well Quantum Confinement Models

We have already made comparison between the two approaches on the their bandgap energy estimations. Now let's discuss on the possible value difference between the two models. Apart from clear bandgap energy estimation difference between the two models, the other valuable result we found from our model (i.e finite potential quantum confinement model) is zero phonon radiative recombination rate that exceed the

value estimated by infinite potential well approximation in the size range below 2 nm diameter of nc-Si. Fig. 2.2 and 2.3 summarize values of zero phonon (psedodirect)and phonon assisted transitions estimated by Hybertsen[9] and Belyakov et al[8] respectively. Based on Belyakov calculations zero phonon transitions follows (R^{-8}) and phonon assisted transition follows (R^{-3}) dependence on dot radius. In most calculation the phonon assisted recombination rates for nc-Si in SiO_2 in diameter do not exceed $10^5 s^{-1}$ and are never less than $10^2 s^{-1}$[8]. For phonon assisted radiative relaxation rate the values we estimated is almost same with the values estimated by infinitely deep quantum well approximation. The major difference is on zero phonon assisted transition rates which are orders of nanosecond below 2nm size for finite potential well approximation. Its value, however, is very small from infinitely deep potential well. Furthermore, both zero phonon and phonon assisted transition do not have faster increment and decrement rates with the variation of size when we compared it with infinitely deep quantum well approximation.

5.5 General Remarks on Exciton and Dielectric Function Effects

All calculations in this paper doesn't include excitonic effect and reduction of dielectric function with the size of sample. The binding energy of exciton is tens of 10^{-3}eV order and is significant at very low temperature. At room temperature its effect is so small that it won't change the general result we already found. However, the variation of dielectric function with size has stronger effect on our decaying rate calculations compared to exciton effect. There is reduction of dielectric function with size. The

prominent effect of this reduction is on the extraction efficiency of the material. Its effect on radiative recombination rate is order of few units. It is important to stress that inclusion of size dependence of dielectric function does affect our result by few units order and its effect is in suppressing it. Inclusion of dielectric function to radiative recombination calculation is straight forward task, what makes it formidable is getting exact size dependent expression for nc-Si inside SiO_2.

Chapter 6

Summary and Conclusion

In this thesis we have presented the bandgap energy , zero phonon and phonon assisted radiative recombination rate based on finite potential and envelope wave function approximation. Furthermore, the results obtained are compared with other calculations based on Infinitely deep quantum well approximation. In our model (finite potential well) the wave function is allowed to spread into SiO_2. Since the wave function is present in two materials, time independent Schrödinger equation is solved in two regions for the envelope function part. Applying matching boundary conditions together with mass discontinuity approximation, we found bandgap energy that substantially deviates from infinitely deep quantum well approximation, particularly in the size range below 5 nm (table 5.1). The bandgap we found are relatively very close to the actual experimental values and values estimated by other better models.

Continuous, square integrable wave function of valence band and conduction band states inside nc-Si is developed in chapter three for envelope wave function part to be used for radiative transition rate calculations. The actual wave function of these electronic states is expanded in band edge Bloch state inside nc-Si, and taken as it is out side nc-Si, as deep level defect state.

Using the wave function we developed, radiative recombination rates for both zero phonon (psedodirect) and phonon assisted transitions are calculated. The momentum overlap factor, which is responsible for direct like radiative transition and the enhancement of phonon assisted process, is again calculated from the envelope function developed by our model. Based on our calculations the momentum overlap of electron and hole is oscillatory function which has significant value at very small size ($\sim 1nm$) and decrease very rapidly to zero as the size increase fig.5.4. Direct radiative transition rate is calculated using Fermi golden rule and life time of nanosecond order in size range 1-2nm (table 5.2) is found and rapidly decreases to zero with oscillating character as we increase size. This is a **new lifetime** estimation which wasn't predicted by infinitely deep quantum well approximation that could explain the blue PL band of oxidized PS and nc-Si embedded inside SiO_2 together with other PL mechanisms. However, phonon assisted transitions are in orders of μs (table 5.3) in size range 1-2 nm and decrease very slowly to their bulk value as we increase size. The values obtained for phonon assisted transitions are almost same with the values found with infinitely deep quantum well approximation.

As a conclusion, the assumption of finite potential well give us an advantage to estimate values at very small size where infinitely deep quantum well approximation is incapable. We are able to develop better bandgap energy estimation using finite potential well approximation. Furthermore, nanosecond lifetime is obtained for size below 2 nm for zero phonon radiative decay rate. However, No new result is found for phonon assisted radiative recombination rates based on our new model that deviates from infinitely deep quantum well approximation.

Appendix A

Appendix

A.1 Programs Used to Solve Bandgap Energy, Momentum Overlap Factor, Direct and Indirect Radiative Transition Rates Numerically

Bibliography

[1] E. Kasper, F. Schaffler, T.P. Pearsall. Semiconductors and Semimetals (Academic press, Boston 1991), p. 233

[2] L.T. Canham: Appl. Phys. Lett. **57**, 1046 (1990)

[3] J. Lin, G.Q. Yao, J.Q. Duan and G.G. Qin: Solid state communications, Vol **97**, No 3, 221 (1996)

[4] L. Pavesi, D.J.Lockwood: Silicon Photonics (Springer-Verlag, Berlin 2004)

[5] J.R. Chelikowsky, M.L. Cohen: Phys. Rev. B **14**, 556 (1976)

[6] G. Ledoux, O. Guillois, D. Porterat, C.Reynaud, F. Huisken, B. Kohn, V. Paillard: Phys. Rev. B **62** 15942 (2000)

[7] V. Ranjan, V.A. Singh, G.C.John: Phys. Rev. B **58**, 1158 (1998)

[8] V.A. Belyakov, V.A. Burdov, R. Lockwood, A. Merdrum: Advances in Optical Technologies, article ID 279502 (2008)

[9] M.S. Hybertsen: Phys. Rev. Lett. **72**, 1514 (1993)

[10] P.M. Fauchet, L.Tsybeskov, C. Peng, S.P. Duttagupta, J.V. Behren, Y. Kostoulas, J.M.V. Vandyshev and K.D. Hirschman: IEEE Journal Of Selected Topics in Quantum Electronics, vol **1**, No 4, 1126 (1995)

[11] N. Koshida, H. Koyama: Ptoelectronics-Devices and Technologies, vol **7**, No 1, PP 103-115(1992)

[12] C.L. Harris, M Syväjärvi,JP Bergman, O Kordina, A Henry, B. Monemar and E. Janzén: Appl. Phys. Lett, **65**, 2451 (1994)

[13] L. Tsybeskov, JV Vandyshev and PM Fauchet: Phys. Rev. B, **49**, 7821 (1994)

[14] G.G Qin, G. Qin: Phys. Stat. Sol. **182**, 335, (2000)

[15] G. Qin, G.G. Qin: J. Appl. Phys. **82** (5) 2572 (1997)

[16] G.G. Qin, Y.J. Li: Phys. Rev. B **68**, 085309 (2003)

[17] M.V. Wolkin, J. Jorne, P.M. Fauchet, G. Allan and C. Delerue: Phys. Rev. Lett. **82**, 1, 197 (1998)

[18] E. Lioudakis, A. Othonos, G.C. Hadjisavvas, P.C. Kelires, A.G. Nassiopoulou: Physica E **38** 128-134 (2007)

[19] Y.Kanemitsu: Phys. Rev B, **48**, 12357 (1993)

[20] S.S. Rink, D.A.B. Miller, D.S. Chemla: Phys. Rev. B **35**, 8113 (1986)

[21] H.G. Yoo, P.M. Fauchet: Phys. Rev. B **77**, 115355 (2008)

[22] O.J. Glembocki, F.H. Pollak: Pyhys. Rev. B **25**, 1193 (1982)

[23] Karl W. Boer: *Survey of Semicondutor Physics*,(1990)

[24] A. Thränhardt, C. Ell, G. Khitrova, and H. M. Gibbs: Phys. Rev. B, **65**, Article ID 035327 (2002)

[25] Arfken, Weber: Mathematical methods for physisits, 5th edition, page 375,377,925 (2001)

[26] M.A. Stroscio,M. Dutta: Phonons in Nanostructures, Cambridge University Press (2004)

[27] J.Singh: Electronic and Optoelectronic Properties of Semiconductor Structures, Cambridge University Press (2003)

[28] Y. kanemitsu, T. Futagi, T. Matsumoto, and H. Mimura: Phys. Rev. B, **49**, 14732 (1994)